

Effective method for high-throughput manufacturing of ultrafine fibres via needleless centrifugal spinning

Huanhuan Chen, Huaizhong Xu, Jiaqi Sun, Chen Liu, Bin Yang

The Key Laboratory of Advanced Textile Materials and Manufacturing Technology, Zhejiang Sci-Tech University, HangZhou 310018, People's Republic of China
E-mail: yangbin665959@gmail.com

Published in Micro & Nano Letters; Received on 4th August 2014; Revised on 27th October 2014; Accepted on 30th October 2014

A nozzle-free spinneret with a flow controller was applied to produce nanoscale fibres of both polymeric solutions and melts by centrifugal field. This centrifugal processing strategy can be used to fabricate non-woven webs composed of fibre diameters ranging from several microns down to 400 nm or less. The fibre morphology and diameter in melt needleless centrifugal spinning (NCS) can be controlled by varying the rotation speed, temperature, liquid properties and collector system. Solution NCS adds the operating parameters of the solution concentration and the solvent. The field emission scanning electron microscope images show that the average diameter of the fibres is approximately $2 \pm 0.8 \mu\text{m}$ and $400 \pm 100 \text{ nm}$ for polyethylene terephthalate fibres (2400 rpm, 245°C) and polyvinylpyrrolidone fibres (20 wt%, 4000 rpm), respectively.

1. Introduction: Centrifugal spinning [1, 2] is a simple and versatile method for generating ultrathin fibres, owing to the fact that no high voltage is required, the high production rate [3, 4] and the wide variety of suitable materials [5, 6]. Centrifugal spinning has been recognised as a promising method for the development of micro- and nanoscale functional devices [7, 8]. The products of centrifugal spinning have shown broad potential applications in the areas of energy, environment and bioengineering [9–12] in which well-aligned architectures, interconnected pores and highly porous properties are a concern. However, recent centrifugal spinning is under research compared with other techniques of ultrafine fibre preparation such as electrospinning and melt blowing. Much attention has been paid to the development of nozzle centrifugal spinning [13–15]. Generally, the strategy of improving the production of nanofibres is mainly based on increasing the number of nozzles and rotational speed. Although the yield is significantly higher than any lab scale electrospinning apparatus, the productivity of which is typically 0.1–1.0 g/h [16, 17], the production is still limited compared with melt blowing method [18]. Furthermore, the problem of nozzles clogging retarded the development of centrifugal spinning because of the superfine nozzles, scale ($<200 \mu\text{m}$) and the high viscosity of the polymeric fluid [19]. Therefore, increasing the output of centrifugal spinning and resolving the clogging problem becomes a concern before it can be industrialised [20]. Recently, a nozzle-free centrifugal spinning method was developed by Weitz *et al.* [2], who put the drops of a polymer solution onto a standard spin coater. Without using a needle nozzle, a number of jets could be emerged from the edge of the flat disk. This method offers a novel and attractive route to centrifugal spinning for the efficient, simple and nozzle-free fabrication of ultrafine fibres, but there still remain some challenges during the processes; for example, the diameter of the fibres fabricated by this method is not uniform, varying from 25 nm to 5 μm , and the morphology of the fibres is hard to control as the exterior forces acting on the jets are unstable.

Inspired by the work of Weitz *et al.*, we report a novel needleless centrifugal spinning (NCS) set-up using a rotating spinning disk with a flow controller as the spinneret. We have demonstrated that a large number of jets can be generated simultaneously on the edge of the spinning disk. The throughput of this approach was about 5 g/min at 2700 rpm for melt spinning. A schematic of

this high-throughput NCS equipment is presented in Fig. 1. It consists of four major components: a nozzle-free rotating spinneret, a ring heater, a direct-current (DC) motor and a circular receiver. Here, the spinneret is designed as a rotating spinning disk (100 mm in diameter and 25 mm in height) with a flow controller which is fixed at the centre of the disk. Multiple rectangular grooves with a width of 2 mm and height of 1 mm are uniformly distributed around the bottom of the flow controller. In the present set-up, the speed of the DC motor can be varied from 500 to 12 000 rpm by a speed controller. The flow controller is designed to control the flow rate and reduce the impact of air on the polymer liquid properties.

2. Experiments: In this study, we focused on the formation of polyethylene terephthalate (PET) and polyvinylpyrrolidone (PVP) fibres, which can be regarded as a prototype system for other NCS melts and solutions. Fig. 2 shows the products as the results of PET melt spinning and PVP solution spinning. During the

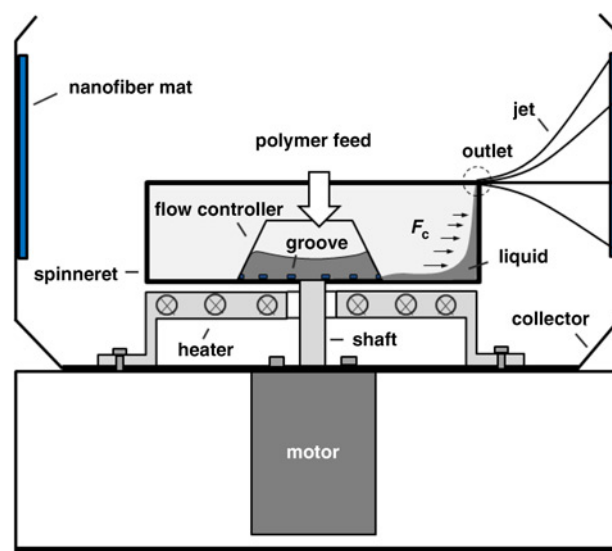


Figure 1 Schematic of the NCS system

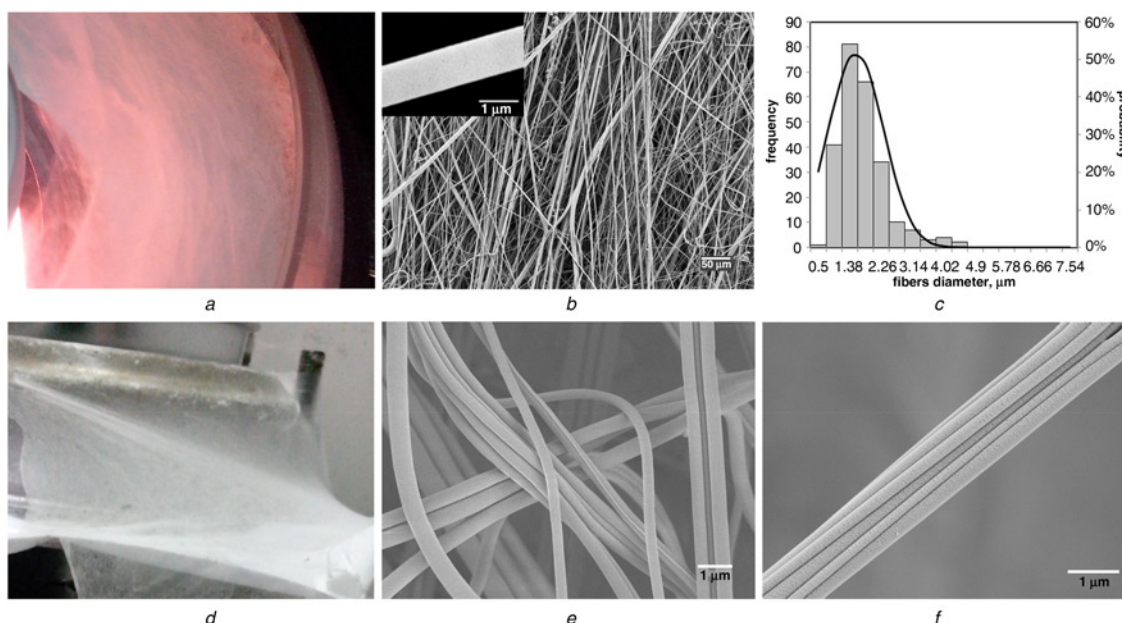


Figure 2 Information on fibres produced by NCS

- a* Image of PET melt spinning at 2700 rpm and 250°C after a one-minute cycle run
b FESEM image of PET fibres
c Diameter distribution for PET fibres
d 20 wt% PVP solutions in water spun at 4000 rpm for 5 min
e FESEM image of PVP fibres
f PVP fibre bundle

melt spinning, PET particles were placed in the liquid controller and the temperature was controlled by a ring heater. Once the desired melting temperature of PET was reached, NCS melts were carried out at 1800 rpm for 2–5 min. After a while, a large number of PET fibres were collected via a circular collector (Fig. 2*a*). The field emission scanning electron microscope (FESEM) image of the PET fibres showed that the fibres were aligned with a uniform diameter and smooth surface (Fig. 2*b*), and the average diameter of the PET fibres was approximately 2 µm in most cases (about 250 measurements using ImageJ 2x software), as shown in Fig. 2*c*. Unlike NCS melts, which require cooling of polymeric jets, NCS solutions employ the characteristics of solvent evaporation to form fibres. As a result, the NCS solution has higher sensitivity to the solution concentration, relative humidity (RH) of air, solvents and rotation speed. To fabricate PVP fibres, 20 wt% PVP solutions in water were used and the experiments were carried out at 4000 rpm, while the RH was kept below 40%.

After 5 min, the PVP fibres were oriented in a random manner and formed a three-dimensional (3D) fibre web, as shown in Fig. 2*d*. The FESEM image showed that the average diameter of the PVP fibres was close to 500 nm, as shown in Figs. 2*e* and *f*.

3. Results and discussion: A general process of fibre formation based on NCS is shown in Fig. 3, which involves: (i) jet initiation from the slits of the liquid controller, (ii) polymer liquid generation towards the inside wall of the disk and thin film formation, (iii) multi-jet production from the film and jet ejection from the edge of the disk, (iv) jet extension to the surface area of the polymer jets and (v) polymer liquid crystallisation until polymer jet solidification and shrinking. Polymer melts or solutions are first ejected from the slits of the liquid controller by rotation. Then, the liquid is drawn to the inside wall of the spinning disk after overcoming the friction of the disk wall and surface tension. Here, the liquid travels in a straight trajectory

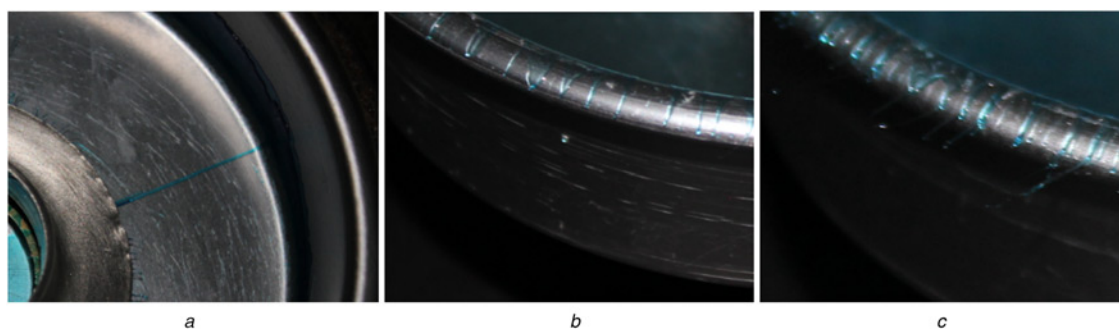


Figure 3 NCS-based fibre formation process

- a* Straight liquid trajectory
b Multi-jet source forming
c Slender jets existing on the edge of the rotating spinning disk and jet diameter reduction
 (Here a 20 wt% PVP solution with blue dye was used and the equipment parameters were adjusted to obtain jets with a large diameter because ultrafine jets were difficult to capture with a high-speed camera.)

Table 1 Experimental results at different rotational speeds for PET melts by centrifugal spinning

Setting temperature, °C	Actual temperature, °C	Rotational speed, rpm	Real speed, rpm	Average fibre diameter, µm	Std. dev, µm
250	255	1500	1505	—	—
250	253	1800	1823	1.63	1.02
250	249	2100	2143	1.26	0.84
250	245	2400	2383	1.55	0.89
250	247	2700	2790	1.06	1.60

relative to the disk coordinate system caused by tangential acceleration at a near-zero level (Fig. 3a). Concurrently, a liquid film is formed on the inside wall of the spinning disk and starts to climb until reaching the edge of the disk (Fig. 3b). When the liquid film leaves the disk, the friction of the wall disappears and multiple jets are created by gas–liquid interface instability [21] (Fig. 3c). Then, the diameters of the jets at the outlet of the spinneret start to decrease until the jets reach a stable size. It is also during this period that a multitude of continuous fibres form between the spinneret and the collector. Finally, a well-aligned fibrous web is produced on the collector. Compared with electrospinning, the NCS technique can provide higher yields of well-aligned ultrafine fibres because of the non-existence of whipping and non-axisymmetric instabilities [22].

The morphology of the fibres prepared by this technique was jointly determined by the polymer properties (surface tension and viscoelasticity), rotational speed, temperature and collector distance, which have a strong influence on jet stretching. The action of the preceding factors on fibre formation can be explained by the Plateau-Rayleigh instability and Matsui model [23]. According to Weitz's and Mahalingam's reports, the formation of jets in this work was similar to Rayleigh–Taylor instability. Under the centrifugal field, the interface between the liquid film and the air was unstable, which led to radial deformation; soon after that, the liquid film turned into an array of cone-shaped jet sources. Along the tangential direction, the polymer liquid at the gas–liquid interface would develop into a wave profile. The wavelength of the unstable wave, that is, the mean distance between the jet sources, was determined by the centrifugal force per volume ($\rho\omega^2 R\partial h/\partial r$) and surface tension per volume ($\gamma\partial^3 h/\partial^3 r$), where ω is the rotational speed, R is the radius of the spinneret, ρ is the density of the polymer liquid, γ is the liquid–air surface tension, h is the height of the liquid film hanging on the edge of the disk and r is the distance of the liquid from the centre of the disk in cylindrical coordinates. Then, the characteristic length of instability could be expressed as $L = (h\gamma/(\rho\omega^2 R))^{1/3}$. According to this formula, a higher rotational speed would result in a shorter characteristic length, which might lead to jet twists with thicker jets and easier breakup into droplets. While at a lower rotational speed, a longer characteristic length would be obtained and no sufficient centrifugal force would be generated to overcome the viscosity of the polymer liquid, which would cause the formation of thicker fibres or no jet creation.

The fibre formation was further illustrated by investigating the influence of air friction. Generally, the jets with a uniform diameter are the result of a dynamic equilibrium between the viscous force F_η and the drag force F_d , which is the resultant force of the centrifugal force and air friction. This rough balance will be unsteady as a consequence of unstable air friction, with which inhomogeneous jet diameters and fibres with a necklace-like structure will result [21]. It is worth noting that with the increase of the jet length, this instability will be enhanced. Interestingly, this instability phenomenon did not continue for long because of the change of flow rates in the positions of the jet sources, which would establish a new balance between viscous and drag forces to restrain the instability of the jets. The relationship between the fibre's diameter and the air friction factor (C_f) can be obtained according to the Matsui model

[24–26]: $C_f = 0.91 (N_{Re})^{-0.61}$, where $N_{Re} = d\rho_a v/\eta_a$. Among the parameters, d , v and ρ_a are the jet's diameter, air velocity and air density, respectively; η_a is the viscosity of air and N_{Re} is the Reynolds number of air relative to the fibre. Assuming that $C_f = 1$, $\rho_a = 1.18 \text{ kg m}^{-3}$, $\eta_a = 26.1 \text{ µPa s}$ and $v = 15.7 \text{ m s}^{-1}$ (3000 rpm), the PET fibre diameter was predicted to be approximately 1.49 µm.

The temperature and rotational speed had strong effects on the formation of fibres. Previous work has demonstrated that the viscosity and surface tension of the polymer liquid are sensitive to the temperature, especially for melts [1]. If the temperature was high, the viscosity of jets was reduced, resulting in the formation of thinner fibres before crystallisation. However, at a low temperature, the viscosity of the jet would be increased and the fibre drawing force might not be enough to form thin fibres, which led to the formation of thicker fibres. With the rotation speed considered, the jet could not move out of the edge of the disk at low angular velocity because of the joint effects of surface tension, air friction and gravity. When a critical rotational speed ($\Omega_1 = 1800 \text{ rpm}$) was reached, the polymer liquid arrived at the edge of the disk and formed multiple jets. When the rotational speed continued to increase, the diameter of the jet began to decrease significantly until it reached an optimum value. Meanwhile, the angular velocity arrived at its second critical speed (Ω_2), which led the jets to form ultrafine fibres. The data collected for PET NCS in Table 1 indicates that fine fibres would be produced at a temperature of 245°C and angular velocity of 2400 rpm.

It is interesting to note that the products with different diameters generated an uneven distribution in the vertical direction in NCS because of the action of aerodynamic forces. Through measurement, we found that the fibre diameters in the upper portion of the webs were smaller than in the lower portion, which was as a result of the centrifugal force, aerodynamic force, gravity and surface tension. The surface tension caused jet instability and bead formation. Under the influence of gravity and aerodynamic force, the beads were distributed at the bottom of the collector and ultrafine fibres were located in the upper position of the collector. This interesting phenomenon has shown that uniform ultrafine fibres could be obtained from the upper portion of the mats. The FESEM images revealed that the bead contents of the resulting fibres decreased significantly after the upper-position fibres in the collector were collected.

4. Conclusion: We demonstrated that nanofibres of polymeric solutions and melts could be produced in this method, and addressed the mechanism of fibre formation in this Letter. In addition, the effects of the rotational speed and temperature of this system on fibre properties were discussed. The FESEM images showed that the average diameters of PET (2400 rpm, 245°C) and PVP (20 wt%, 4000 rpm) fibres were approximately $2 \pm 0.8 \text{ µm}$ and $400 \pm 100 \text{ nm}$, respectively. The proposed set-up could be utilised to develop fibres for various materials, which could be used in applications such as tissue engineering, energy storage, filtration and membrane science.

5. Acknowledgments: The authors gratefully acknowledge the Open Foundation of Textile Sciences and Engineering level

subjects (grant no. 2014KF02), which enabled them to begin research on centrifugal spinning of nanofibers. Parts of this work (SEM) were carried out in the College of Materials and Textiles, ZheJiang Sci-Tech University.

6 References

- [1] Shanmuganathan K., Fang Y., Chou D.Y., *ET AL.*: 'Solventless high throughput manufacturing of poly (butylene terephthalate) nanofibers', *ACS Macro Lett.*, 2012, **1**, (8), pp. 960–964
- [2] Weitz R.T., Harnau L., Rauschenbach S., Burghard M., Kern K.: 'Polymer nanofibers via nozzle-free centrifugal spin-ning', *Nano Lett.*, 2008, **8**, (4), pp. 1187–1191
- [3] Raghavan B., Soto H., Lozano K.: 'Fabrication of melt spun polypropylene nanofibers by force spinning', *J. Eng. Fabrics Fibers (JEFF)*, 2013, **8**, (1), pp. 52–60
- [4] Wang L., Shi J., Liu L., *ET AL.*: 'Fabrication of polymer fiber scaffolds by centrifugal spinning for cell culture studies', *Microelectron. Eng.*, 2011, **88**, (8), pp. 1718–1721
- [5] Reneker D.H., Yarin A.L.: 'Electrospinning jets and polymer nanofibers', *Polymer*, 2008, **49**, (10), pp. 2387–2425
- [6] Rutledge G.C., Fridrikh S.V.: 'Formation of fibers by electrospinning', *Adv. Drug Deliv. Rev.*, 2007, **59**, (14), pp. 1384–1391
- [7] Li Q., Sun X., Lozano K., *ET AL.*: 'Facile and scalable synthesis of 'caterpillar-like' ZnO nanostructures with enhanced photoelectrochemical water-splitting effect', *J. Phys. Chem. C*, 2014, **118**, (25), pp. 13467–13475
- [8] Badrossamay M.R., McIlwee H.A., Goss J.A., *ET AL.*: 'Nanofiber assembly by rotary jet-spinning', *Nano Lett.*, 2010, **10**, (6), pp. 2257–2261
- [9] Desai K., Kit K., Li J., *ET AL.*: 'Nanofibrous chitosan non-wovens for filtration applications', *Polymer*, 2009, **50**, (15), pp. 3661–3669
- [10] Senthilram T., Mary L.A., Venugopal J.R., *ET AL.*: 'Self crimped and aligned fibers', *Mater. Today*, 2011, **14**, (5), pp. 226–229
- [11] Huang J., Virji S., Weiller B.H., *ET AL.*: 'Polyaniline nanofibers: facile synthesis and chemical sensors', *J. Am. Chem. Soc.*, 2003, **125**, (2), pp. 314–315
- [12] Amalorpava Mary L., Senthilram T., Suganya S., *ET AL.*: 'Centrifugal spun ultrafine fibrous web as a potential drug delivery vehicle', *Express Polym. Lett.*, 2013, **7**, pp. 238–248
- [13] Sarkar K., Gomez C., Zambrano S., *ET AL.*: 'Electrospinning to force-spinning™', *Mater. Today*, 2010, **13**, (11), pp. 12–14
- [14] McEachin Z., Lozano K.: 'Production and characterization of polycaprolactone nanofibers via forcespinning™ technology', *J. Appl. Polymer Sci.*, 2012, **126**, (2), pp. 473–479.
- [15] Padron S., Patlan R., Gutierrez J., *ET AL.*: 'Production and characterization of hybrid BEH-PPV/PEO conjugated polymer nanofibers by forcespinning™', *J. Appl. Polymer Sci.*, 2012, **125**, (5), pp. 3610–3616
- [16] Padron S., Fuentes A., Caruntu D., *ET AL.*: 'Experimental study of nanofiber production through forcespinning', *J. Appl. Phys.*, 2013, **113**, (2), p. 024318
- [17] Dosunmu O.O., Chase G.G., Kataphinan W., *ET AL.*: 'Electrospinning of polymer nanofibres from multiple jets on a porous tubular surface', *Nanotechnology*, 2006, **17**, (4), p. 1123
- [18] Zuo F., Tan D.H., Wang Z., Jeung S., Macosko C.W., Bates F.S.: 'Nanofibers from melt blown fiber-in-fibre polymer blends', *ASC Macro Lett.*, 2013, **2**, (4), pp. 301–305
- [19] Bell N.S., Missert N.A., Garcia R.M., *ET AL.*: 'Surface engineering of electrospun fibers to optimize ion and electron transport in Li% 2B battery cathodes' (Sandia National Laboratories, 2012)
- [20] Mo X.M., Xu C.Y., Kotaki M., *ET AL.*: 'Electrospun P (LLA-CL) nanofiber: a biomimetic extracellular matrix for smooth muscle cell and endothelial cell proliferation', *Biomaterials*, 2004, **25**, (10), pp. 1883–1890
- [21] Mahalingam S., Edirisinghe M.: 'Forming of polymer nanofibers by a pressurised gyration process', *Macromol. Rapid Commun.*, 2013, **34**, (14), pp. 1134–1139
- [22] Ajao J.A., Abiona A.A., Chigome S., *ET AL.*: 'Electric-magnetic field-induced aligned electrospun poly(ethylene oxide) (PEO) nanofibers', *J. Mater. Sci.*, 2010, **45**, (9), pp. 2324–2329
- [23] Gupta V.B., Kothari V.K.: 'Manufactured fiber technology' (Chapman & Hall, London, 1997), p. 573
- [24] Chen C.H., White J.L., Spruiell J.E., *ET AL.*: 'Dynamics, air drag, and orientation development in the spunbonding process for nonwoven fabrics', *Textile Res. J.*, 1983, **53**, (1), pp. 44–51
- [25] Matsui M.: 'Air drag on a continuous filament in melt spinning', *Trans. Soc. Rheol. (1957–1977)*, 1976, **20**, (3), pp. 465–473
- [26] Shambaugh R.L.: 'A macroscopic view of the melt-blowing process for producing microfibers', *Ind. Eng. Chem. Res.*, 1988, **27**, (12), pp. 2363–2372